

Lab Report

**S261: Optical Astronomy and Gravitational
Lensing**

Chenhuan Wang and Harilal Bhattacharai

September 24, 2020

1. Lensing

1.1. Background*

1.1.1. Cosmic Expansion

A spatially homogeneous and isotropic Universe can be described as FLRW metric. Solving Einstein's field equations with FLRW metric gives expansion of the Universe [2]. Hubble parameter $H(t) = \dot{a}(t)/a(t)$ evolves according to

$$H^2(t) = H_0^2 [\Omega_{\text{rad}} a^{-4}(t) + \Omega_{\text{mat}} a^{-3}(t) + \Omega_{\text{curv}} a^{-2}(t) + \Omega_\Lambda] \quad (1.1)$$

Because of expansion of the Universe, light emitted in the past gets redshifted over time. The redshift of a source is given by,

$$z = \frac{\lambda_{\text{obj}} - \lambda_{\text{em}}}{\lambda_{\text{em}}} \quad (1.2)$$

Where, λ_{obs} and λ_{em} are, respectively, the wavelengths at time of observation and emission. Redshift is directly related to the scale factor by,

$$1 + z = \frac{1}{a(t_{\text{em}})} \quad (1.3)$$

with scale factor at present time defined as $a(t_0) = 1$. Also, this equation shows that the Universe was half of its current size when a source at redshift $z = 1$ is observed.

The local Hubble law is given by the following formula,

$$v_{\text{esc}} = H_0 D \quad (1.4)$$

where, $H_0 = H(t_0)$ is Hubble constant and D is the distance between object and observer.

1.1.2. Distances

Accordingly, one defines the angular diameter distance as exactly this ratio,

$$D_{\text{ang}}(z) = 2R/\delta = a(z)f_K(w) \quad (1.5)$$

Where, R is the radius of the distant object, δ is the angular diameter, and z is the cosmological redshift. If we consider an observer at redshift z_1 gives the angular diameter of another object at redshift z_2 , so equation 1.5 becomes

$$\begin{aligned} D_{\text{ang}}(z_1, z_2) &= a(z_2)f_K[w(z_2) - w(z_1)] \\ &= \frac{1}{1+z_2} f_K \left[\frac{c}{H_0} \int_{z_1}^{z_2} \frac{dz'}{\sqrt{(1-\Omega_m-\Omega_\Lambda)(1+z')^2 + \Omega_m(1+z')^3 + \Omega_\Lambda}} \right] \end{aligned} \quad (1.6)$$

*Content taken from [1], if not noted otherwise.

Another distance measure relates the observed flux, S , of a source to its luminosity, L . For a known luminosity, the distance to the source can be determined as,

$$D_{\text{lum}}(z) = \sqrt{\frac{L}{4\pi S}} \quad (1.7)$$

1.1.3. Quasars

Quasars (QUASi-stellar radio sources) are an extremely luminous and distant active galactic nuclei(AGN). The power for AGNs comes from accretion of matter onto super-massive black-hole, where the significant fraction of the gravitational energy is released as radiation. The radiating part of the quasars must be very compact due to the variability nature [1]. Quasars have variable luminosity at shorter wavelength which can be used to determine the time delay between light beams.

1.1.4. Gravitational lensing

A gravitational field is caused by distribution of the matter like, a cluster of galaxies between distant light source and an observer. Due to the effects of this field, light rays are bending traveling from a source to an observer. This effect is called the *gravitational lensing*. The general situation of gravitational lensing is considered as in figure.1.1 Where, we suppose the mass distribution at distance D_d , a source is located at distance D_s , and D_{ds} is the distance from deflector to a source. All distances used in gravitational lensing are the angular diameter distances.

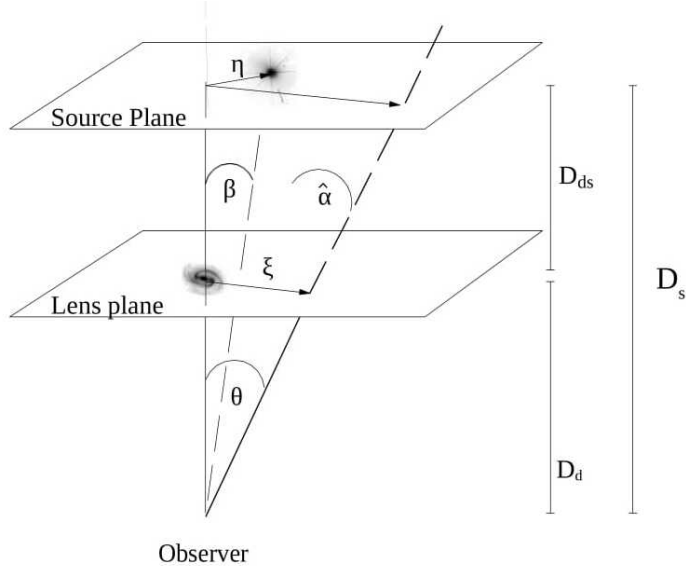


Figure 1.1.: schematic diagram of a gravitational lensing [1].

Lens Equation

To study the deflection of light by mass distribution, called lens system, we consider some conditions. First, the distance from an observer to lens and lens to a source is very large so we assume that all angles considers are small i.e. $\tan x \approx \sin x \approx x$. Secondly, source

plane and lens plane are parallel, and deflection of light only occur in lens plane as in Bonn approximation. For a given source, the lens equation is given by,

$$\boldsymbol{\beta} = \boldsymbol{\theta} - \boldsymbol{\alpha}(\boldsymbol{\theta}) \quad (1.8)$$

where, $\boldsymbol{\theta}$ is the apparent angular position of the source in the sky, $\boldsymbol{\beta}$ is its true position, and $\boldsymbol{\alpha}$ is the scaled deflection angle.

The scaled deflection angle and true deflection angle are connected as,

$$\boldsymbol{\alpha}(\boldsymbol{\theta}) = \frac{D_{ds}}{D_s} \hat{\boldsymbol{\alpha}}(D_d \boldsymbol{\theta}) \quad (1.9)$$

Now, we can define a dimensionless surface mas density with convergence as,

$$\kappa(\boldsymbol{\theta}) = \frac{\sum(D_d \boldsymbol{\theta})}{\sum_{cr}} \quad (1.10)$$

with the critical surface mass density,

$$\Sigma_{cr} = \frac{c^2}{4\pi G} \frac{D_s}{D_d D_{ds}} \quad (1.11)$$

The scaled deflection angle can be written purely in terms of observable angles as,

$$\boldsymbol{\alpha}(\boldsymbol{\theta}) = \frac{1}{\pi} \int d^2\theta' \kappa(\boldsymbol{\theta}') \frac{\boldsymbol{\theta} - \boldsymbol{\theta}'}{|\boldsymbol{\theta} - \boldsymbol{\theta}'|^2} \quad (1.12)$$

For further convenience, a deflection potential is introduced

$$\psi(\boldsymbol{\theta}) = \frac{1}{\pi} \int d^2\theta' \kappa(\boldsymbol{\theta}') \ln |\boldsymbol{\theta} - \boldsymbol{\theta}'| \quad (1.13)$$

The use of this quantity is well-motivated because it encloses all information of the mass distribution of the lens [1]. In addition, relation of deflection potential and deflection angle can be found

$$\boldsymbol{\alpha}(\boldsymbol{\theta}) = \nabla \psi(\boldsymbol{\theta}) \quad (1.14)$$

From the deflection potential a further scalar function, the Fermat potential, can be defined

$$\tau(\boldsymbol{\theta}; \boldsymbol{\beta}) = \frac{1}{2} (\boldsymbol{\beta} - \boldsymbol{\theta})^2 - \psi(\boldsymbol{\theta}) \quad (1.15)$$

Finally to find the magnification of the images is given by

$$\mu = (det A)^{-1} \quad (1.16)$$

where, A is the Jacobian matrix of lens mapping.

$$A_{ij} = \frac{\partial \beta_i}{\partial \theta_j} \quad (1.17)$$

Strong lensing

Multiple images of a source can be obtain in strong lensing. It can be describe by considering the Format potential $\tau(\beta; \theta)$ with fixing β and assuming $\det A \neq 0$ [1].

- Minima: $\det A > 0, \text{tr } A > 0$
- Maxima: $\det A > 0, \text{tr } A < 0$
- Saddle points: $\det A < 0$

Critical curves and Caustics: Those points in image plane where the magnification diverges i.e. $\det A = 0$ called critical curves. Also, the mapping of a critical curve into the source plane is called caustics. In general, critical curves are closed and smooth. Caustics are closed, but not necessarily smooth.

The Odd Number Theorem

If a source has a large offset from line of sight from observer to the lens, it is easy to see only one image. The odd number theorem describe as: when we started with one image there will always be an odd number of images of gravitational lensing; however, normally at least one of them is highly de-magnified. So, we can observe only even number of images mostly as doubly or quadruply [1].

The SIS (Singular Isothermal Sphere)

A simple model to describe the mass distribution of a galaxy acting as a lens is the singular isothermal sphere (SIS):

$$\rho(r) = \frac{\sigma_v^2}{2\pi Gr^2} \quad (1.18)$$

where σ_v is the velocity dispersion. Physically this means that the lens system consists of self-gravitating with Maxwellian velocity distribution [3].

Integration along the line of sight yields the surface mass density

$$\Sigma(\xi) = \frac{\sigma_v^2}{2G\xi} \quad (1.19)$$

A characteristic angular scale of an axisymmetric lens is given by the Einstein radius θ_E , defined as the angle inside which the mean of the convergence is unity. As a consequence, the projected mass inside θ_E can be written as [1],

$$M(\theta \leq \theta_E) = \pi \theta_E^2 D_d^2 \Sigma_{cr} \quad (1.20)$$

We use it to determine the mass of the lensing galaxy. For an SIS the Einstein radius can be calculated as [1],

$$\theta_E = 4\pi \left(\frac{\sigma_v}{c} \right)^2 \frac{D_{ds}}{D_s} \quad (1.21)$$

1.1.5. Time Delay

We have described about multiple images on the topic strong lensing. Light rays of different images have different paths from source to observer, thus there can be different travel times. There are two different contributions of time delay. First one is geometric time delay and second is the potential time delay which induced by the way of light through a gravitational potential [1].

We will find the time delay by using the following expression [1]

$$c\Delta t(\beta) = (1 + z_d) \frac{D_d D_s}{D_{ds}} [\tau(\boldsymbol{\theta}_A; \beta) - \tau(\boldsymbol{\theta}_B; \beta)] \quad (1.22)$$

here, $\boldsymbol{\theta}_A, B$ are the positions of the two images. Equation 1.22 shows that the time delay is proportional to the inverse Hubble constant, i.e.

$$\Delta t \propto \frac{1}{H_0} \quad (1.23)$$

In this experiment we can use *minimum dispersion method* to calculate time-delays. The light curve for one quasar image is denoted as $A(t_k)$ and other one is $B(t_k)$ which is shifted by time shift λ . In this case, the dispersion function D^2 is defined as [1],

$$D^2(\lambda, \Delta m) = \sum_{k=1}^N (A(t_k) - B(t_k + \lambda, \Delta m))^2 \quad (1.24)$$

where, the light curves are sampled at a discrete number of times t_k . This method basically search for minimal dispersion in 2d-plane of λ and Δm . The error bars of the time delay can be estimated by a Monte-Carlo strategy.

1.1.6. Calibration frames

In astronomical observation, the different kind of calibration frames are necessary for image reduction. These frames are described as following.

BIAS

An empty CCD (Charge Coupled Detector) has still get positive numbers due to DC offset that is added in the electronics and A/D converter. In addition there is read out noise present. This is called bias [1]. A BIAS frame is obtained by taking exposure of no exposure time with shutter closed and the image read out of unexposed CCD.

DARK

The main purpose of dark frame is to measure the dark current (thermal noise). The dark frames are made by taking expose time equal to the largest exposure time of science frame with shutter closed [1].

FLAT

All the pixels of CCD have different quantum efficiency (QE), so they need to be properly normalized. One way to obtain a flat field frame is by illuminating the telescope dome from the inside and taking short exposures as not to saturate the CCD. It is called dome flats and they can always obtain even during daytime. Another way is by sky flats which are obtained by taking exposures during evening and/or morning twilight [1].

1.1.7. Image reduction

The image reduction is done to remove instrumental signature and improve the signal-to-noise (S/N) in the data before extracting any scientific information[1].

Super-flat and Fringing

If the flat frame unable to flatten the pixels properly then we should use super-flat. The position of the telescope is slightly displaced every time, dithering, to avoid the same region of the sky falling on to the pixels. It also correct the falling of important data on bad pixels in the image. Science exposures should be used for a super-flat frame [1].

If the variations in the science frame are multiplicative, then the science frame have to be divided by the super-flat. However, if the variation are additive, then we get a fringe pattern which is subtract by de-fringing model. These fringes mainly occur on a CCD image from monochromatic light due to interference. Since fringing is an additive effect so it must be subtracted from the science frame. Fringe model is obtained by smoothing the super-flat with large number of pixels and subtracted from the science images to obtain fully corrected images for pixel-to-pixel variations [1].

Masking and Weighting

During the analysis of data, bad pixels cause problems that lead incorrect result. It can be assigning these pixels by a certain value. Then these values recognised by the software programs and neglect them. The mask file contain information about the exposure time which turns them into weight image [1].

Astrometric Calibration

The mapping between image co-ordinate and sky co-ordinate. It should done with the help of catalog, so we use reference catalog on-line (SDSS-R9). Then the astrometric solution is calculated by using Scamp software package [1].

Sky Subtraction

Along with the target object CCD also collects light from background sky. This has to be removed from the image to get only the flux from the object of interest. To do so, first, we have to remove all the objects in the frame and image has to be smoothed with a specific kernel width. The background image is subtracted from the original frames [1].

Co-adding

Stacking all science frame in to one master frame is called Co-adding. One needs to make sure that each objects should fall onto the same pixel. This leads to the high S/N values than individual frames [1].

Photometric Calibration

The earth atmosphere play an important role in our observations. Different telescopes have different flux values for the same target in different atmospheric conditions. For standard stars, the relation between instrumental magnitude and true magnitude is given by [1],

$$m_{\text{calb}} = m_{\text{instr}} + Z \quad (1.25)$$

Where Z is the photometric zero point.

1.2. Preparatory Tasks

P.3.1 Calculation of the deflection potential, $\psi(\theta)$ and the scaled deflection angle of an SIS lens.

From equation 1.13 the deflection potential, which gives the information about the mass distribution of the lens, is define as,

$$\psi(\theta) = \frac{1}{\pi} \int d^2\theta' \kappa(\theta') \ln |\theta - \theta'| \quad (1.26)$$

In the case of axial symmetry of SIS lens equation 1.13 simplifies to (given on the question)

$$\psi(\theta) = 2 \int_0^\theta d\theta' \theta' \kappa(\theta') \ln \left(\frac{\theta}{\theta'} \right) \quad (1.27)$$

By substituting the values of $\Sigma(D_d\theta)$, where $D_d\theta = \xi$ from equation 1.19 and Σ_{cr} from equation 1.11 on equation 1.10, then by plugging the new expression of $\kappa(\theta)$ equation 1.27 becomes

$$\begin{aligned} \psi(\theta) &= \frac{4\pi}{c^2} \frac{D_{ds}}{D_s} \sigma_v^2 \int_0^\theta d\theta' \ln \left(\frac{\theta}{\theta'} \right) \\ &= \frac{4\pi}{c^2} \frac{D_{ds}}{D_s} \sigma_v^2 \left[\theta' \ln \left(\frac{\theta}{\theta'} \right) + \theta' \right] \\ &= \theta_E (\theta \ln \theta - \theta \ln \theta + \theta) \end{aligned}$$

Therefore,

$$\psi(\theta) = \theta_E \theta \quad (1.28)$$

From equation 1.14 scaled deflection angle is defined as

$$\alpha(\theta) = \nabla \psi(\theta) \quad (1.29)$$

From equations: 1.28 and 1.29,

$$\alpha(\theta) = \nabla \theta_E \theta = \theta_E \hat{\theta} \quad (1.30)$$

P.3.2: Solving the lens equation and finding the separation between images

The lens equation is given by,

$$\beta = \theta - \alpha(\theta) \quad (1.31)$$

By using the expression for scaled deflection angle for SIS from 1.30

$$\beta = \theta - \theta_E \hat{\theta} \quad (1.32)$$

or,

$$\alpha(\theta) = \beta + \theta_E \hat{\theta}$$

for $\hat{\theta} > 0$,

$$\theta_A = \beta + \theta_E$$

for $\hat{\theta} < 0$,

$$\theta_B = \beta - \theta_E$$

Thus, the separation of these images is given by,

$$\Delta\theta = \theta_A - \theta_B = 2\theta_E \quad (1.33)$$

P.3.3: Magnification ratio of the two images of SIS lens.

The magnification of a gravitational lens is given by,

$$\mu = (\det A)^{-1} \quad (1.34)$$

P.3.4: Time delay derivation for SIS lens as a function of θ_A and θ_B .

The time delay is given by[1]

$$c\Delta t(\beta) = (1 + z_d) \frac{D_d D_s}{D_{ds}} [\tau(\theta_A; \beta) - \tau(\theta_B; \beta)] \quad (1.35)$$

Also, from 1.15 the Format's potential is defined as,

$$\tau(\theta; \beta) = \frac{1}{2}(\beta - \alpha)^2 - \psi(\theta) \quad (1.36)$$

So,

$$\tau(\theta_A; \beta) = \frac{1}{2}(\beta - \theta_A)^2 - \psi(\theta_A) \quad (1.37)$$

By plugging the values of β and $\psi(\theta_A)$,

$$= \frac{1}{2}(\theta_A - \theta_E - \theta_A)^2 - \theta_E \theta_A \quad (1.38)$$

Therefore,

$$\tau(\theta_A; \beta) = \frac{1}{2}\theta_E^2 - \theta_E \theta_A \quad (1.39)$$

Similarly,

$$\tau(\theta_B; \beta) = \frac{1}{2}(\beta - \theta_B)^2 - \psi(\theta_B) \quad (1.40)$$

$$= \frac{1}{2}(\theta_B + \theta_E - \theta_B)^2 - \theta_E \theta_B \quad (1.41)$$

$$\tau(\theta_B; \beta) = \frac{1}{2}\theta_E^2 - \theta_E \theta_B \quad (1.42)$$

By substituting these values equation 1.35 becomes,

$$c\Delta t(\beta) = (1 + z_d) \frac{D_d D_s}{D_{ds}} \left(\frac{1}{2}\theta_E^2 - \theta_E \theta_A - \frac{1}{2}\theta_E^2 + \theta_E \theta_B \right) \quad (1.43)$$

Therefore,

$$\Delta t(\beta) = \frac{(1 + z_d)}{c} \frac{D_d D_s}{D_{ds}} \theta_E (\theta_B - \theta_A) \quad (1.44)$$

Thus, the time delay is proportional to the Einstein radius.

P.3.5: Minimum Dispersion Estimator

The minimum dispersion estimator is a simple, efficient and well tested method to estimate time delay from observed light curve[1] It helps to fine the difference between the curve at various delay times. Since it assume that light curves have the same shape but they are separated by time.

P3.6: The approximation of dispersion function near the minimum by a parabola.

The dispersion function near the minimum can be find by Taylor expanding of the functional function. i.e.

$$d^2(\lambda) = D^2(\lambda_0) + \frac{dD^2(\lambda_0)}{d\lambda}(\lambda - \lambda_0) + \frac{d^2D^2(\lambda_0)}{d\lambda^2}(\lambda - \lambda_0)^2 + 0 \quad (1.45)$$

Where, D^2 is the dispersion function and λ is the time shift. Here high order terms are negligible compared to first and second order terms.

The dispersion function is minimum at $\lambda = \lambda_0$. Now the second term of equation 1.45 goes to zero. i.e.

$$d^2(\lambda) = D^2(\lambda_0) + \frac{d^2D^2(\lambda_0)}{d\lambda^2}(\lambda - \lambda_0)^2 \quad (1.46)$$

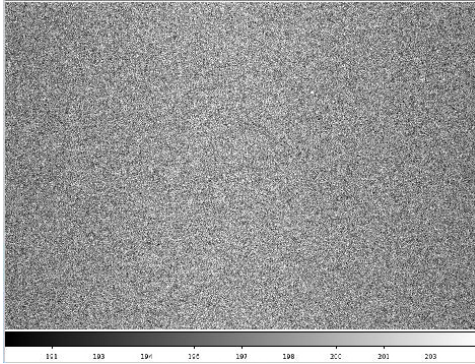
it is parabolic in shape.

1.3. Image reduction

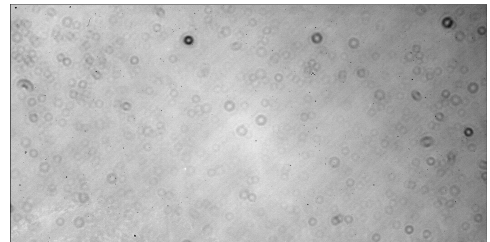
Calibration frames and science frames have been already taken. Dark frames are not provided and not necessary, since dark currents can be neglected in this case due to proper cooling. Here these images will get inspected and reduced as explained before.

1.3.1. Raw-image inspection

Calibration images are firstly visually inspected using `ds9` with `zscale` setting. Figure 1.2a and 1.2b are examples of bias and flat frames. Note that images shown here are not the whole images.



(a) Bias frame



(b) Flat frame. Color legend was unfortunately not included in screenshot.

Figure 1.2.: Calibration frames. Shown images are only central part of whole images.[†]

Average bias level is somewhat near 200. This values changes, though not so obvious in figure 1.2a, throughout the image. Left and right sides are significantly darker, meaning less bias. Presumably it is related to geometry and layout of CCD chip. Sometimes one can see quite large white dots in bias picture. Positions of these white dots vary from image to image. Because of its significant size comparing to other noises, they are mostly likely to be cosmic rays, as hinted by [1].

Middle of bias frame is chosen to calculated background and sigma, due to its lack of large-scale variation. Output of `imstats` gives us mean and sigma: 198.72 ± 2.59 . Noise here should be readout variations and random fluctuations [1].

In flat-field, most obvious feature is black circles or doughnuts. These are dusts on dewar windows and/or filter [1]. This results in lower photon counts, thus black in flat-field images. They are not on CCD chips, since they are not properly focused. Some large-scale structure can be seen. It can be explained by different quantum efficiency at different area of CCD. There are quite a lot small sharp black dots visibly. They are most likely to be bad pixels and dust directly on CCD chip.

Each flat-field has different exposure time. One can try to find correlation between mean value of image and exposure time using commands provided in [1]. Ratios between these two goes down with increasing exposure time. Firstly of all, CCD chips should be saturated here,

[†]Unfortunately some images were taken without the color/gray scale.

since with exposure time, mean values goes down. One possibility is that read-out noise in circuit gets averaged out with long exposure time, thus lower ratio.

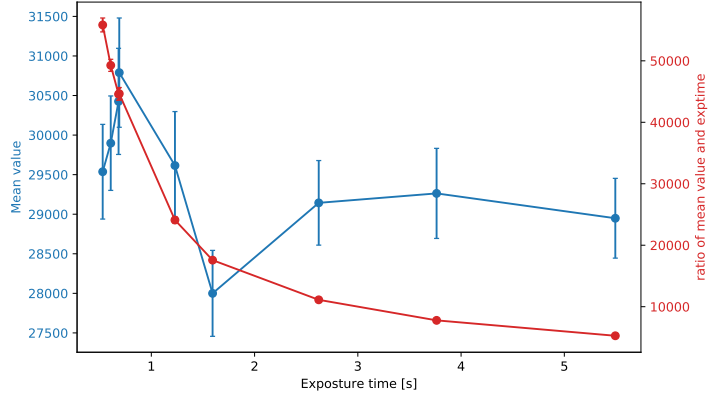


Figure 1.3.: Mean values (red) with sigmas and the ratios (blue) against exposure time of flat-field images.

In science frame one can clearly see doughnut structures and sharp black dots as in flat-field frames. Between exposure, most out-standing change would be that telescope is moving around.

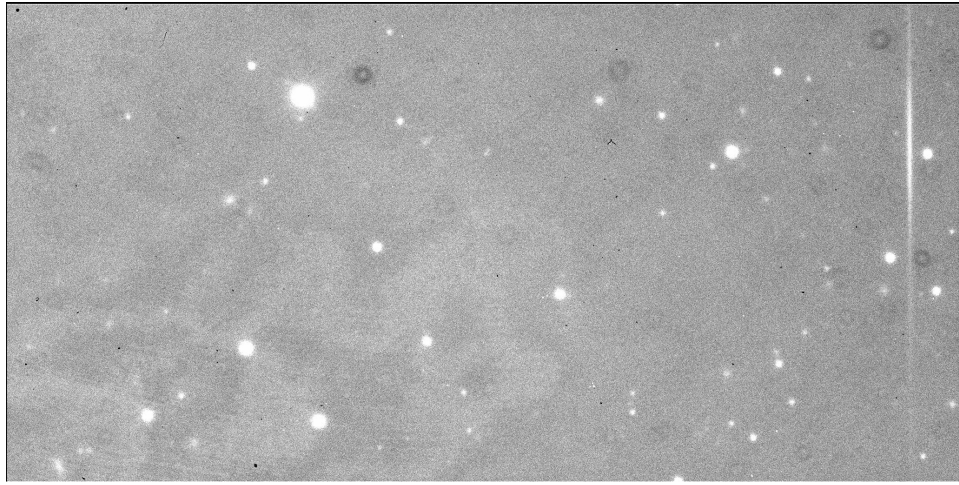


Figure 1.4.: An example of science frame.

We use `image008068.fits` as an example and compute mean and sigma in area without bright objects. Values are 693.20 ± 19.00 . It is greater than the mean value of bias frame. This is easy to understand, since science frame must contain sky.

1.3.2. Image reduction

Several science frames containing source SDSS1650+4251 are taken from one filter (R). Now these images will be reduced with help of calibrations frames and some more in `theli`. `theli` mainly consists of several tabs or processing groups. Each of following paragraph corresponds one processing group/

Initialise First off, `theli` should be properly reset and initialised. Number of CPU cores and instrument (telescope) are specified accordingly. Paths containing bias, flat, and science frames are filled in.

Preparation Through this processing group, headers contained in `.fits` files can be split and/or corrected. Comparison of headers before and after corrections reveals

- size in x and y are swapped, meaning orientation of images has been changed,
- (useless) information, e.g. comments, CCD info, Date, and etc., has been removed,
- lots of lines starting with DUMMY have been added.

They are more changes, but the listed alterations are most noticeable.

Calibration In this step, calibration frames are getting co-added. In co-addition process, images are stacked on top of each other, while making sure each object falls onto the same pixel [1]. By doing this and in the end only calibrating with co-added images, random noises will get averaged out.

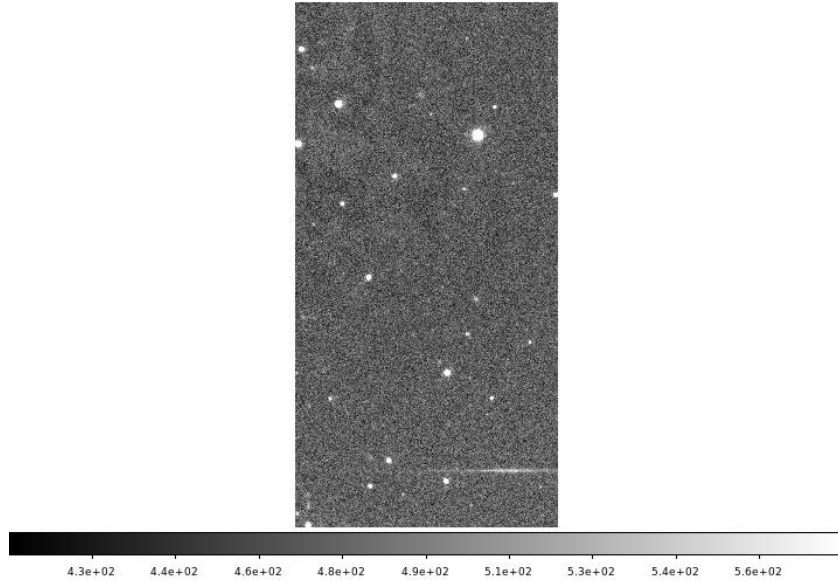
After co-addition, bias frames are free of small white dots as seen before and flat frames get a bit brighter. One can further compute noise dispersion of co-added bias frame and single bias frame. They are respectively 0.72 and 2.27. So noise level in co-added images is much lower.

The minimal value in normalised flat-field is 0. Dithering during co-addition helps to remove bright objects (stars and etc.).

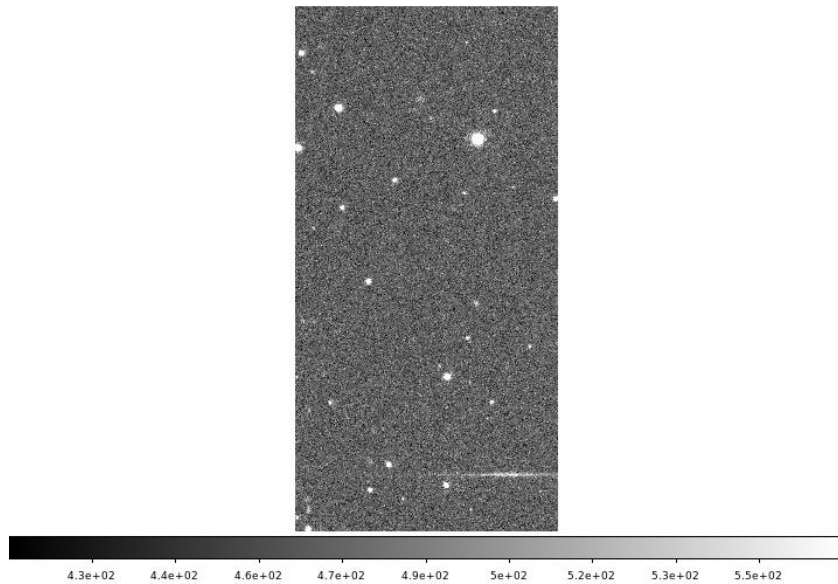
Background modelling In this processing group, only background model correction is selected, where a super-flat and fringe model is created and applied. Its configurations are set according to [1]: DT = 1.0, DMIN = 10, mask expansion factor= 3, median combination, divide smoothed model, subtract fringes method, smoothing kernel for background model = 256.

In super-flat, one can clearly see fringes pattern. Fringes and background sky can be extracted with smoothing process. In `SDSS1650+4251_R_block0_1_fringe.fits`, there is only fringes visible and in `SSD1650+4251_R_block0_1_illum.fits` only smooth gradient, i.e. background.

Correction given by illumination is roughly 500 (counts). Fringes are removed after correction, see figure 1.5a and 1.5b.



(a) Before correction. Pay attention to top left corner.



(b) After correction. Pay attention to top left corner.

Figure 1.5.: Background modelling

Weighting In this step, weighting and masking are performed to compensate bad pixels and different quantum efficiency. Global weights and WEIGHTS are created and applied.

Astrometry/Photometry This processing group matches dithered frame to standard astrometric coordinates and performs photometry calibration. Astrometric reference catalog is retrieved using setting provided in [1]: `Web(france)`, `SDSS-DR9`, `mag limit9|`, `radius=5'`. 421 objects are found. Then detection threshold is set to 2σ and minimal area for detection of

10 pixels.

Matching is done with `Scamp` with `DISTORT_DEGREES=1`. Calculation is done after `Scamp` has been correctly configured. After this, numerous check plots are generated.

Co-addition Frames are astrometrically co-added, subtracted by sky/background, and normalised to exposure time of 1 s. Settings are again provided in [1]: `Model the sky`, `DT=1`, `DMIN=10`, `kernel width=256`, outlier rejection to 4. After co-addition, newly generated frames can be found in new folder with name starting with `coadd_`, see figure 1.6. Logically, they have the same shapes and brightest region of co-added weight frame also has high S/N ratio. Indeed, one can compute noise using `imstats` as before. RMS of region free off bright objects is 0.02, far lower than previous single frames. This can be properly understood, since frames are co-added and then normalised, resulting high S/N ratio.

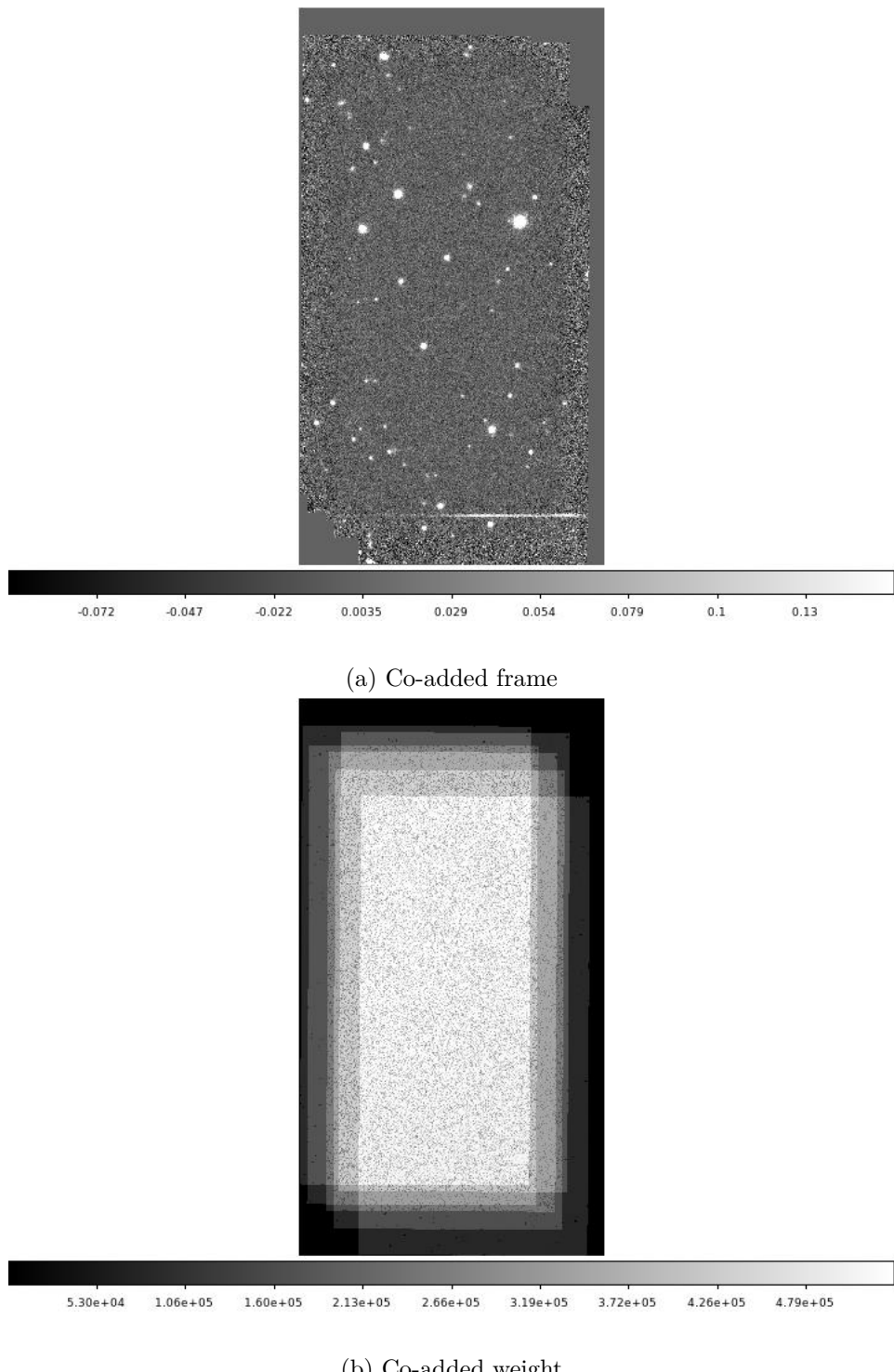


Figure 1.6.: Frames generated after co-addition

1.4. PSF extraction

In this section, point-spread-function (PSF) will be extracted. First of all, the target need to be found using standard coordinates: RA = $16^{\text{h}}50^{\text{m}}43.4^{\text{s}}$, DEC = $+42^{\circ}51'49''$.00. In `ds9`, coordinates can be turned on with `coordinate grid` option, see figure 1.7. As mentioned in [1], this target consists of two lensing images, but the separation have similar size as a typical seeing, so images are blended.

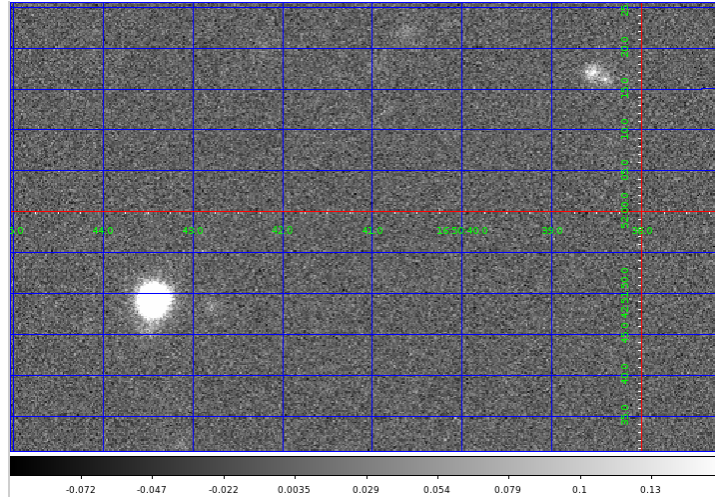
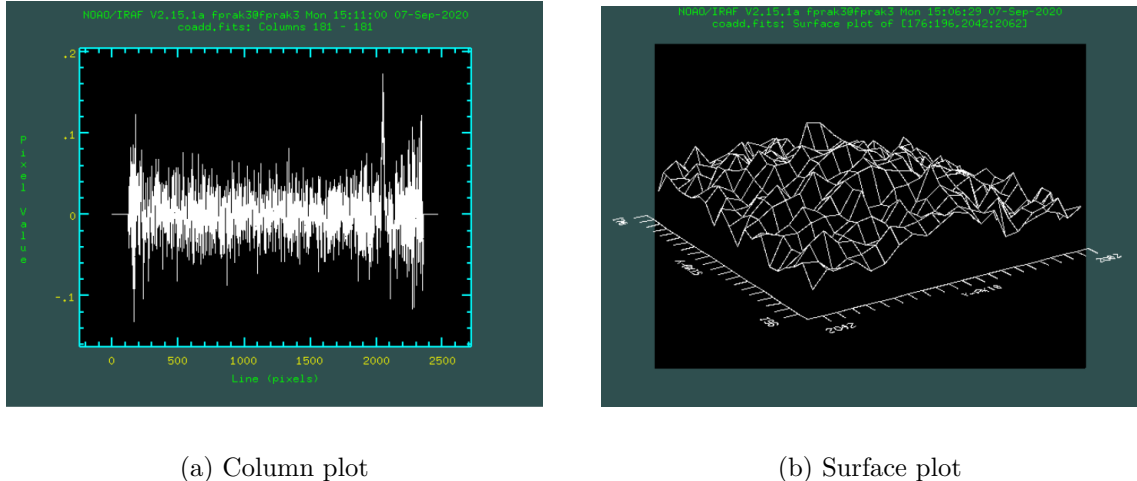


Figure 1.7.: Co-added frame with coordinate grid. Target is the left-bottom bright object.

In order to perform component fitting, PSFs of other various objects need to be extracted. One can gain more detailed information about objects using `iraf` task `imexam`.



(a) Column plot

(b) Surface plot

Figure 1.8.: Example plots of a galaxy

There are mainly two categories of objects: stars and galaxies. Since galaxies contain a number of radiation sources, their full widths at half maximum (FWHMs) are typically larger than single stars. Indeed, that is what we see. FWHMs of stars are $\sim 6 \pm 1$ pixels, of galaxies $\sim 9 \pm 1$ pixels. Identification of stars and galaxies can be easier with various plots provided by

imexam. Two example plots each are figure 1.8 and 1.9. In contour plots, stars appear to be (almost perfect) concentric circles while galaxies are messier. Radial profiles of star have clear trend while they are scattered for galaxies. These plots support previous argument regarding differentiation stars from galaxies. [seeing in arcseconds?](#)

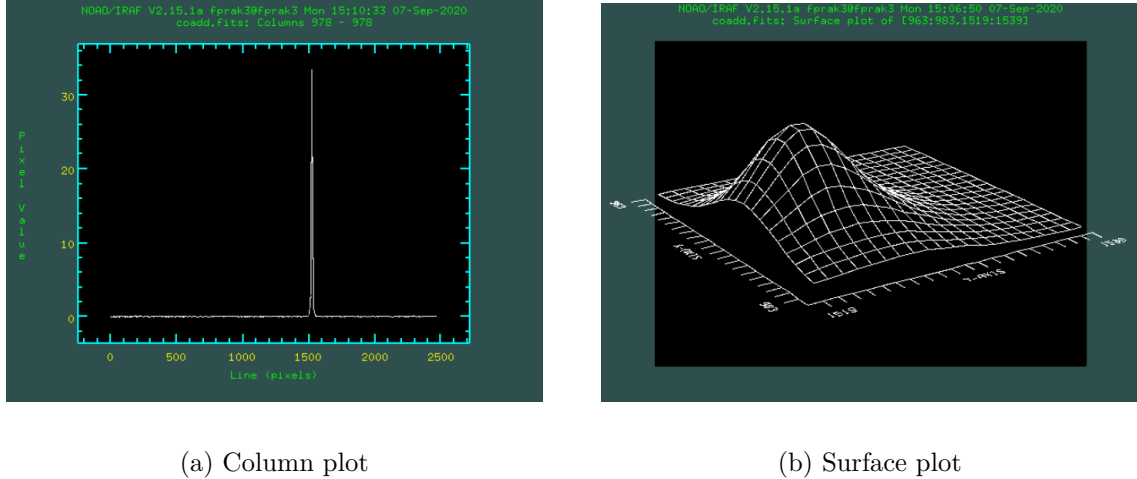


Figure 1.9.: Example plots of a star

Target contains two images, so its FWHM lies in between stars and galaxies at 8.71 pixels. Plots of target appear a bit different as well, see figure. 1.10. While surface plot do have some rough edges, column plot gives us the definite answer that this objects contains two images.

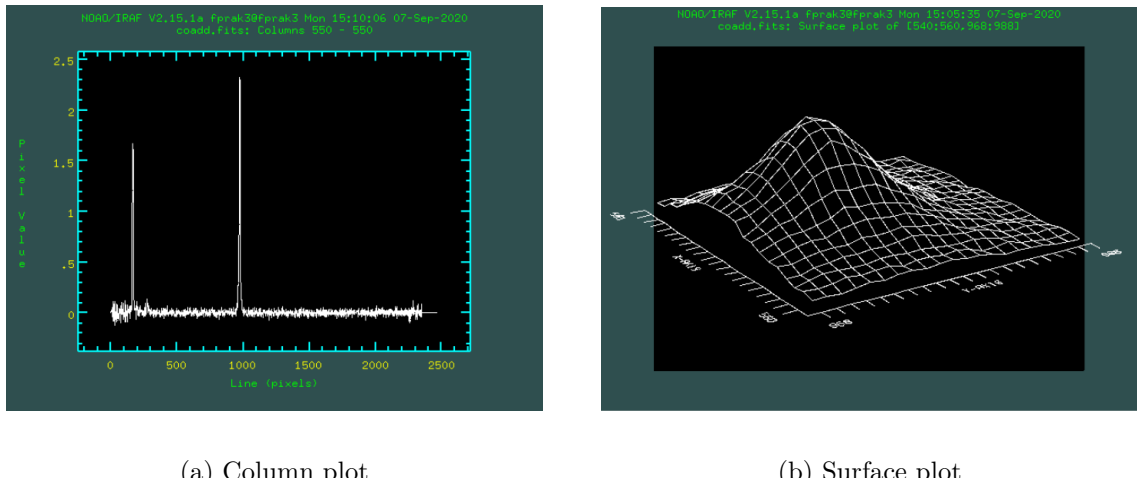
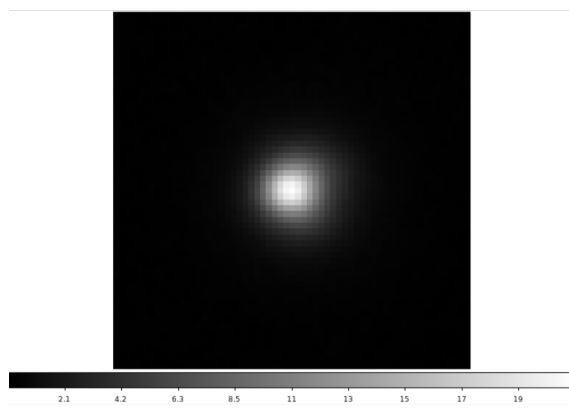


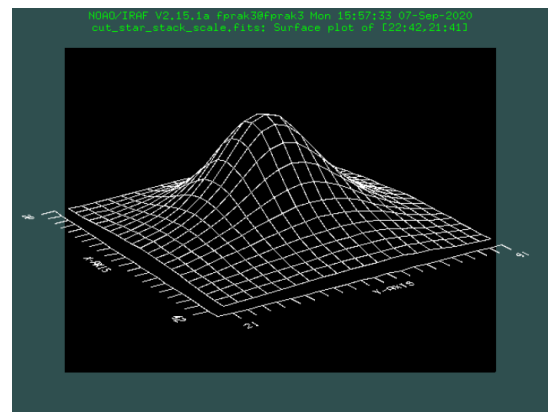
Figure 1.10.: Example plots of the target

Now to extract PSFs, a csh shell script `create_psf.csh` is used. The script takes four inputs: DIR the directory containing the images, LIST containing outputs of `imexam` of selected stars and the target, RADIUS size of square getting cut, and MAX_FWHM_STACK the maximal size of PSF. One needs to use stars, since they are quasi-point-like sources. Stars brighter (higher flux) than the target need to be included in LIST. [Why?](#) RADIUS is set to 30 pixels and MAX_FWHM_STACK to 8.5. LIST file can be found in A.1.

Outputs of `create_psf.csh` are each individual cut-outs `cut_scale*.fits` and stacked PSF `cut_star_stack_scale.fits`. Inspection of `cut_star_stack_scale.fits` shows that there is no contribution from neighbouring stars, see figure 1.11b. MFWHM of the stacked image is 8.09 as expected. Its surface plot is quite a smooth hump, even smoother than the hump of a single star. In the subsequent component fitting, the stacked image will be used, since all fluctuations/errors are averaged out.



(a) The Stacked image in ds9



(b) Surface plot of stacked image

1.5. Component fitting

Although two images are blended, one can still try to use component fitting to find out individual flux and their separation. The 2d fitting program `galfit` is used here.

`galfit` is able to fit sky value in images and sky background is important to compute the σ -image [4]. Sky value is a fit parameter in `galfit`, thus one need to compute it using `imstats` and `dfits` for normalisation: $\text{sky}=1.71 \text{ s}^{-1}$. This value is then added into the image with `ic` command provided in [1].

Input parameters of fitting are stored in `galfit.input`, listed in appendix A.2. Most important things are positions of two images, relative magnitude. These are just rough estimates as initial guess. Sky background is the third component of the fitting and sky ADU counts from previous part are given as input.

Execution of component fitting with the given parameter list outputs a log file `fit.log` and a image block, see figure 1.12. The log file contains the coordinates of two images

$$\mathbf{r}_A = (29.69 \pm 0.05, 24.71 \pm 0.08), \quad \mathbf{r}_B = (31.11 \pm 0.01, 31.16 \pm 0.01)$$

magnitude difference 1.70, and $\chi^2_\nu = 44.542$. From the residuals, one can see that the fitting works properly. They are quite uniformly distributed with some fluctuation, except there is a slightly bright spot at bottom. As suggested by the tutors, it could be caused by neighbouring stars.

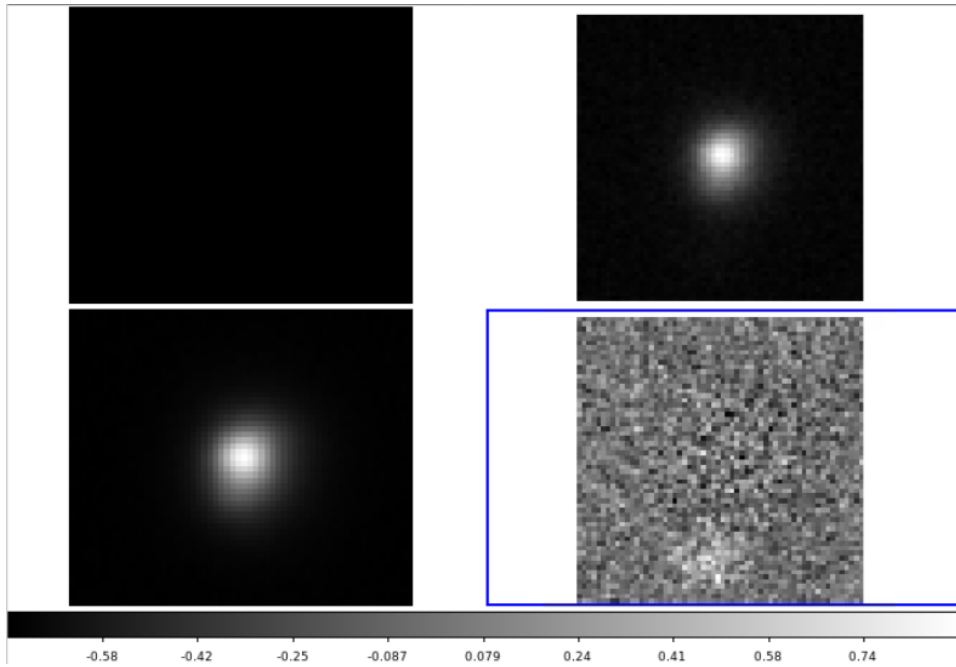


Figure 1.12.: The image block generated by `galfit` assuming there are *two* images. First image is intended to be empty. Second and third are respectively original and modelled images. Last one shows the residuals.

One could also wonder if the target could consist only of one image, since it appears to be so visually. Another fitting is done but only with two components, one PSF fit and one sky background. Resultant image block is figure 1.13. There is a clear dark spot in the residual

plot and $\chi^2_\nu = 101.615$, much worse than previous fitting. So the image cannot be explained by just one image.

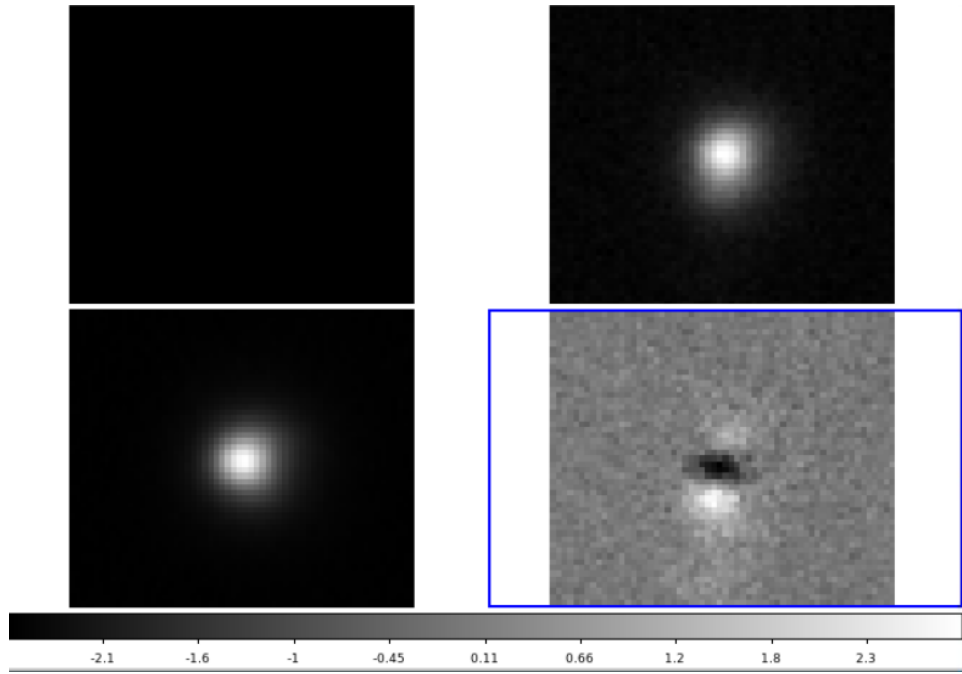


Figure 1.13.: The image block generated by galfit assuming there is only *one* image. First image is intended to be empty. Second and third are respectively original and modelled images. Last one shows the residuals.

1.6. Time-delay estimate

Time delay between two images can be estimated using minimal dispersion method. But a large number of observations are needed for it to work. Thus we take the data of [5] and the raw data are presented in appendix. A.4.

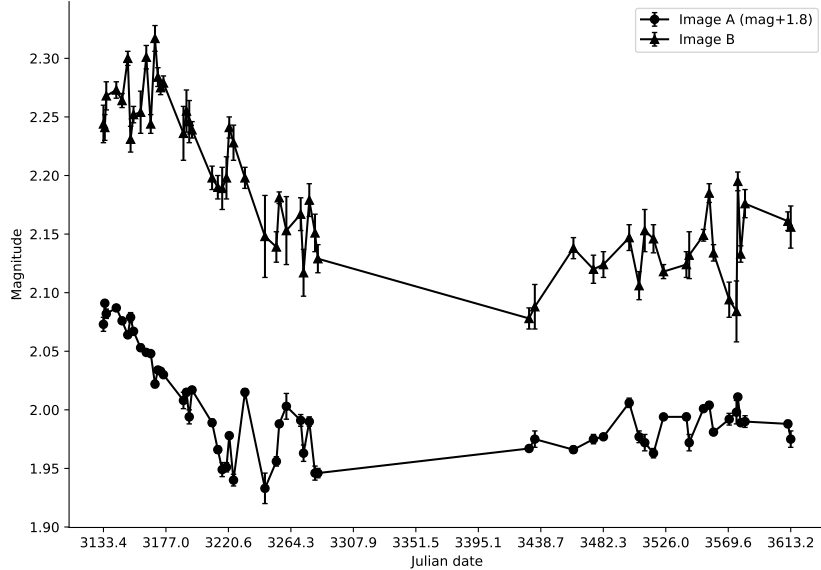


Figure 1.14.: Light curves of two images. Note that image A is originally much dimmer. For better comparison, its magnitude is added with 1.8.

Before using minimal dispersion method, one can try to inspect the light curves visually. Figure. 1.14 shows the light curves. Most noticeable feature is a large gap between observations caused by rotation/spin of the Earth. Time delay is quite hard to discern in this plot, but if there is it should be $\mathcal{O}(10)$ days. There is also quite a magnitude difference.

To reliably determine time delay of two images, one has to use minimal dispersion method, implemented in program `tde1`. Before using Monte Carlo, one should roughly find good input parameters of the program, so that the true global minimum can be found. Parameters are listed in table. A.2.

Time delay is determined to be

$$\lambda = 34.29 \quad (1.47)$$

Dispersion spectra of this preliminary run are figure. 1.15a, 1.15b, and 1.15c. Note the magnitude shift here refers to the magnitude shift after an initial adjustment, so that in the end minimal dispersion should be located at somewhere near zero magnitude shift. Indeed, the dispersion spectra show no clear minima within the selected region, except for zero magnitude shift. So we are certain that we found a global minimum.

With this knowledge and input parameters, Monte Carlo is turned on and it gives us

$$\lambda = 34.336 \pm 2.184 \quad (1.48)$$

Here Monte Carlo method also gives us probabilities of various time delays, see figure. 1.16.

Fitting using function

$$f(t) = \frac{1}{\sigma\sqrt{2\pi}} \exp\left(-\frac{1}{2} \frac{(t - \mu)^2}{\sigma^2}\right)$$

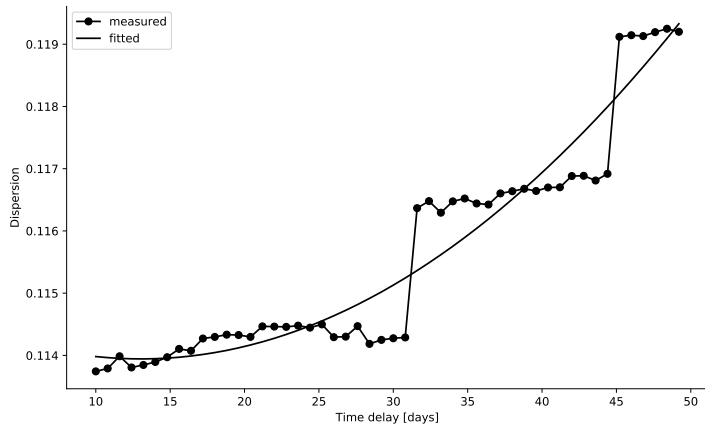
determined the parameters and covariance matrix to be

$$\mu = 33.959$$

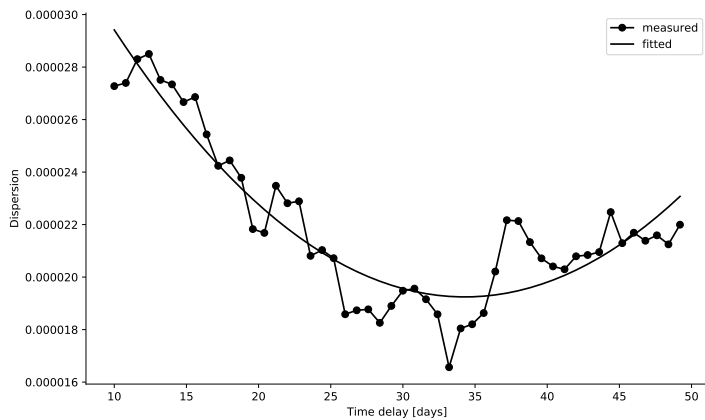
$$\sigma = 1.988$$

$$\Sigma = \begin{pmatrix} 0.0064 & -0.0002 \\ -0.0002 & 0.004 \end{pmatrix}$$

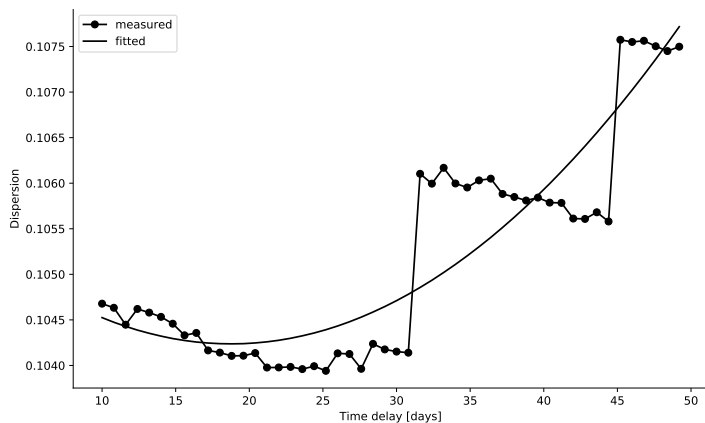
Note that here the fit function does not have either multiplicative or additive constant, since we have probability directly. These values are very close to direct output of Monte Carlo. So one may say the result of Monte Carlo is realistic.



(a) magnitude shift = -2.5



(b) magnitude shift = 0



(c) magnitude shift = 2.4

Figure 1.15.: Dispersion spectra with various magnitude shifts.

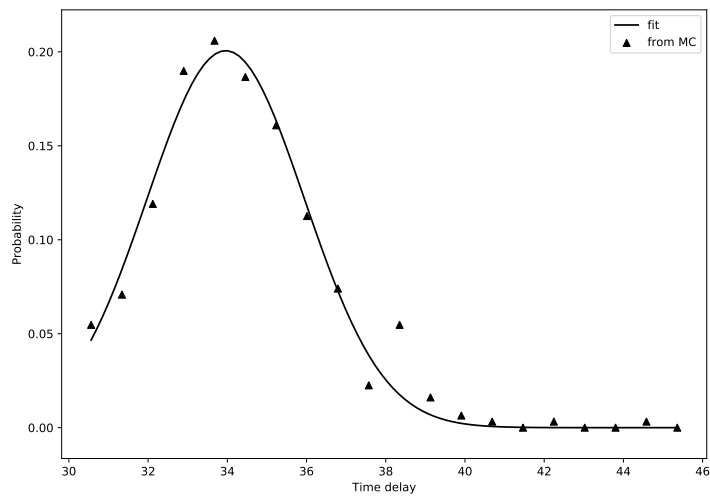


Figure 1.16.: Probability of different time delays estimated by Monte Carlo method. Raw data in appendix. A.6

1.7. Lensing analysis

Calculation with accepted value of H_0 Since the redshifts of lens and source system are known, one can from image separation determine the velocity dispersion in SIS model. Angular distances should be computed also by equation. 1.6. Here the cosmological parameters are taken from [6]

$$\Omega_m = 0.3089 \pm 0.0062, \quad \Omega_\Lambda = 0.6911 \pm 0.0062$$

For simplicity, errors in these parameters are not propagated in further analysis (almost negligible). For this part, currently accepted value of H_0 is used.

Image separation can be used to compute Einstein radius. Results of `galfit` are in pixels, so they need to be converted to angles first. As given in [7], the field of view of Cassegrain focus is $21' \times 14'$, meaning one pixel corresponds to $0.4''$. Image separation can be expressed by Einstein radius with equation. 1.33. The separation in pixels and in radians are then

$$\begin{aligned}\Delta r &= 6.600 \pm 0.079 \text{ (pixels)} \\ \Delta\theta &= (1.281 \pm 0.015) \cdot 10^{-5} = 2\theta_E\end{aligned}$$

Here the error is properly propagated using

$$\begin{aligned}\sigma_{\Delta r}^2 &= \left(\frac{\partial \Delta r}{\partial x_A}\right)^2 \sigma_{x_A}^2 + \left(\frac{\partial \Delta r}{\partial y_A}\right)^2 \sigma_{y_A}^2 + \left(\frac{\partial \Delta r}{\partial x_B}\right)^2 \sigma_{x_B}^2 + \left(\frac{\partial \Delta r}{\partial y_B}\right)^2 \sigma_{y_B}^2 \\ &= \frac{1}{(\Delta r)^2} [(x_A - x_B)^2 (\sigma_{x_A}^2 + \sigma_{x_B}^2) + (y_A - y_B)^2 (\sigma_{y_A}^2 + \sigma_{y_B}^2)]\end{aligned}$$

With equation. 1.21, one finds

$$\sigma_v = (9.913 \pm 0.597) \cdot 10^{-4} c \quad (1.49)$$

where the error is given by

$$\sigma_{\sigma_v} = \frac{\sigma_v}{2\theta_E} \sigma_{\theta_E}$$

According to equation. 1.20, projected mass inside Einstein radius is computed to be

$$M(\theta < \theta_E) = (5.766 \pm 0.139) \cdot 10^{11} M_\odot \quad (1.50)$$

This has similar magnitude as the estimated mass of milky way ($\sim 1 \times 10^{12} M_\odot$) [8]. The error is propagated to be

$$\sigma_M = \frac{2M}{\theta_E} \sigma_{\theta_E}$$

Determination of H_0

2. Bad weather

2.1. Introduction

In this part of this experiment, we can determine the properties of CCD mounted at the telescope. These measurements are carried out at the 50 cm telescope during day-time. But, here, we have just carried out it with already taken data which are provided us by AlFA, Bonn. In this lab, we can measure the dark current and its dependence on temperature, the detector gain and read-out noise, linearity, and full well capacity.

2.2. Background

2.2.1. Observations in Optical Astronomy

The main objective of this section is to understand some facts and concepts about observations in optical astronomy.

Telescope Optics

In our observation we used a 50 cm reflector telescope of the Cassegrain type which is available in AIFA. The incident light from a source first falls on a concave parabolic primary mirror (1) then re-reflected by a hyperbolic convex mirror (2). The rear focus (A) of the secondary is placed in the focus of the primary mirror such that the light is collimated in the convex focus of the secondary mirror (B) via a small hole, which is making without disturbing the focal length of such mirror, in the primary mirror. A detector is placed behind the primary mirror because light rays are collimated at (B). A schematic diagram of this telescope is as shown in Fig. 2.1.

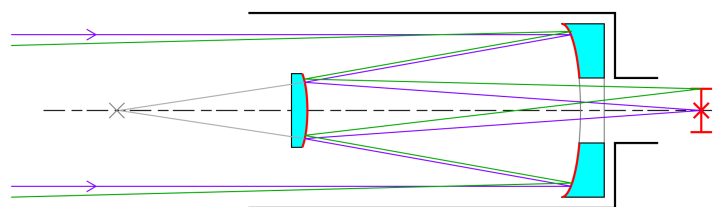


Figure 2.1.: Schematic light path in a Cassegrain telescope[1].

Seeing and Airmass

The earth's atmosphere has been considered as a part of the optical system for ground based astronomical observation. So, numerous effects arise, mostly, turbulence in the atmosphere leads fluctuation on refractive index on short spatial and temporal scale. This results in a blurring and scintillation of the PSF. That complicated shape can be represented by approximately

Gaussian shape in two dimensions. Thus, the full width at half maximum(FWHM) size of the Gaussian shape of such stellar image is called Seeing of the image. It helps to measure the actual resolution in a particular observation. For Bonn, a seeing is 2 arcsec is a best value.

The column density on the atmosphere through which the light travels compared to vertical in-fall is called Airmass. For an angular distance z from zenith the best approximation can be computed as,

$$a = \frac{1}{\cos z} \quad (2.1)$$

Where, $a = 1$ for an object at the zenith i.e. $z = 0^\circ$ and $a = \infty$ at horizon. Thus, the best possible observing position is near the zenith.

Magnitude

In optical astronomy, the optical brightness of a source is called magnitude.

The difference in magnitudes between two sources is defined on the basis of ratio of their observed fluxes S_1 and S_2 as,

$$\Delta m = m_1 - m_2 = -(100^{1/5}) \cdot \log_{10} \left(\frac{S_1}{S_2} \right) \quad (2.2)$$

From definition it is clear the fainter sources have higher magnitude.

Coordinate system

There are different co-ordinate systems (like as equatorial co-ordinate system, galactic co-ordinate system, and etc.) use to quantify the position of celestial objects in optical astronomy. Here, equatorial system is a most common system for identifying and cataloging the sources. In this system the framework of terrestrial latitude and longitude projected from the centre of earth onto the sky.

- Declaration is an analogy to latitude in geography. Here, the north pole having declination of $\delta = 90^\circ$ and projection of south pole is $\delta = -90^\circ$. It is express as degree, minute and second.
- Right Ascension, α , is equivalent to longitude with the equatorial zero point. It is express as hour, minute and second.

2.2.2. CCD Characteristics

CCDs are the composition of essentially pure silicon based two-dimensional pixel detector, so it response wide wavelength range (from near infrared to the soft X-ray). The physical light deflection mechanism involved in a CCD is the photoelectric effect. They have 2D array of light sensitive pixels having size, typically, 10μ to 20μ .

The distribution of photons is converted to a distribution of charge packets which are collected and stored in three dimensional potential wells. To measure the amount of charge in

each packets they have to be transported across the full detector surface to output amplifier. During this transportation of charge packets potential barriers in the transport direction can be manipulated by applying appropriate voltage waveform. The transport is done by parallel shift and series shift. On this functioning principle electrons are shifted, detected and converted in a digital number or count or analog-to-digit unit (ADU) at a rate of about 30 kHz.

The best CCDs have high quantum efficiency, low read noise, and excellent linearity. In this experiment we will determine these properties. Some of these properties are discussed below:

Quantum Efficiency

Quantum efficiency is define as The ratio of produced electrons to the number of photons hitting the detector surface. It is determine by the photon absorbing capacity of silicon in given wavelength. The best CCDs have high quantum efficiency, low read noise, and excellent linearity. In this experiment we will determine these properties. Top order CCDs have the significant wavelength range more than 90%.

Read-Out Noise

An empty CCD, read out have a small scatter in signal level from pixel-to-pixel due to the amplification noise occurring in the electronics. The standard deviation of this scatter is called read out noise. The main sources of amplification noise are size of amplifier, integrated circuit contraction and temperature of amplifier.

Stability

There are several aspect to hold excellent stability characteristic by a CCD. Some of them are:

- CCD is geometrically very stable because it is contracted by pure silicon.
- It keeps its performance over years without degradation.
- It has very high sensitivity; however, very insensitive to over-exposure.

Dark Current

The dark current is a thermal noise which is composed of electrons liberated by thermal energy. It is depend on temperature of CCD. At room temperature it fills CCD pixels to their saturation level within a short period of time (a minute or even less). Therefore, it is necessary to keeps the detector system at a low temperature. The cooing of CCD is done thermo-electrically with closed cycle system or by using liquid nitrogen. It is a less advantageous property of CCDs.

The dark current, I_{dark} (measured in the unit of $e^-/\text{Pix/S.}$) increases exponentially with temperature, T , as

$$I_{\text{dark}} = c \cdot T^{3/2} \cdot e^{-\frac{E_g}{2k_B T}} \quad (2.3)$$

Where, $E_g = 1.16$ eV is the silicon band gap energy, $k_B = 8.62 \cdot 10^{-5}$ eV/K is the Boltzmann constant, and c is a detector specific constant.

Gain

The ratio, k , between the amount of charge in a CCD pixel and the corresponding digital number after A/D conversion is called detector gain. It is measured in the unit of e^-/ADU . It can be derived based on the assumption that photons(or electrons) numbers are explained by Poisson statistics. i.e. in a detector area with constant flat illumination the variance σ_e^2 of the pixel to pixel fluctuation equal to the average number of electrons per pixel N_e .

$$N_e = \sigma_e^2 = kN_{e,d} = k^2\sigma_{e,d}^2 \quad (2.4)$$

Where, $N_{e,d}$ and $\sigma_{e,d}$ are the corresponding numbers after A/D conversion. Therefore, to calculate the gain we have to determine the average signal level and variance in a well exposed area of the detector and using following expression,

$$k = \frac{N_{e,d}}{\sigma_{e,d}^2} \quad (2.5)$$

Noise

Noise always means that the standard deviation of the signal level. In our detector system there are two other noise components in the data which have to be separated. First one is read out noise (RON) and second is pixel-to-pixel fluctuation noise due to different quantum efficiency of different pixels. This is so-called Pixel Response Non-Uniformity (PRNU) noise. Thus, the total noise is given by,

$$\sigma_{tot} = \sqrt{\sigma_{RON}^2 + \sigma_e^2 + \sigma_{PRNU}^2} \quad (2.6)$$

Where, σ_{PRNU} gives small deviation in QE from pixel-to-pixel and it is also directly proportional to N_e given by,

$$\sigma_{PRNU} = N_e f_{PRNU} \quad (2.7)$$

Where, f_{PRNU} is the detector dependent characteristic PRNU factor. It is typically in the order of 0.01.

Linearity and full-well capacity

One the most appealing feature of CCDs as astronomical detectors is their linearity. Here, the output signal is proportional to the incoming photons received by the detector. They are linear over the full dynamic range of 10^4 to 10^5 and deviation from linearity is just $\pm 0.5\%$ for well behaved system.

The CCD pixels have limited charge capacity. The maximum number of the electrons fitting into a single pixel is called full well capacity. It can measure in the unit of e^- . The scientific CCDs have $100000e^-$ full well capacity. If the pixels get full well then the CCD shows blooming effect. Saturation level is the range of a CCD signal, so it is measure in the unit of ADU.

A. Appendix

A.1. LIST file

COL	LINE	RMAG	FLUX	SKY	PIXELS	R	ELLIP	PA	PEAK	MFWHM
293.05	1859.53	19.30	191.3	0.15	80	3.51	0.019	82.5	3.98	7.96
435.95	1647.42	18.24	505.1	0.40	79	3.50	0.011	-63.1	10.49	8.12
974.61	1522.59	16.49	2531.7	2.10	79	INDEF	0.029	-38.3	52.22	8.16
652.00	1365.48	19.99	101.2	0.09	78	2.88	0.056	83.9	2.14	7.93
851.99	603.17	18.72	326.0	0.27	77	1.64	0.022	72.2	6.86	8.20
623.70	265.30	19.54	153.1	0.11	81	4.12	0.022	-13.9	3.18	7.88
279.06	1492.48	18.34	459.4	0.36	80	3.11	0.022	81.2	9.48	8.03
549.09	975.02	19.86	113.3	0.12	75	INDEF	0.015	68.6	2.32	8.71

A.2. galfit.input

```

# IMAGE and GALFIT CONTROL PARAMETERS
A) new_cutscale8.fits                      # Input data image (FITS file)
B) new2_cutscale8.fits                      # Output data image block (FITS file)
C) none                                      # Sigma image name (made from data if blank or "none")
D) cut_star_stack_scale.fits                 # Input PSF image (FITS file)
E) 1                                         # PSF fine sampling factor relative to data
F) none                                      # Bad pixel mask (FITS image or ASCII coord list)
G) none                                      # File with parameter constraints (ASCII file)
H) 0 60 0 60 # Image region to fit (xmin xmax ymin ymax)
I) 100 100                                     # Size of the convolution box (x y)
J) 26.0                                       # Magnitude photometric zeropoint
K) 0.038 0.038                                # Plate scale (dx dy) [arcsec per pixel]
O) both                                       # Display type (regular, curses, both)
P) 0                                           # Options: 0=normal run; 1,2=make model/imgblock & quit
S) 1                                           # Modify/create objects interactively?

```

```

# INITIAL FITTING PARAMETERS
#
# column 1: Parameter number
# column 2: initial gues for value
# column 3: allow parameter to vary (yes = 1, no = 0)
# column 4: comment

```

```

# Component 1:
# PSF fit.

0) psf                                         # object type
1) 30 31 1 1                                  # position x, y [pixel]
3) 16                                         # total magnitude (only relative values are relevant)
8) 1                                           # axis ratio (<=1)
Z) 0                                           # leave in [1] or subtract [0] this comp from data?

```

```

# Component 2:
# PSF fit.

0) psf                                         # object type

```

```

1) 31 31    1 1      # position x, y [pixel]
3) 18          1      # total magnitude (only relative values are relevant)
8) 1          0      # axis ratio (<=1)
Z) 0          0      # leave in [1] or subtract [0] this comp from data?

# Component 3:
# sky background

0) sky          # object type
1) 1.71         1      # sky background [ADU counts]
2) 0.000        0      # dsky/dx (sky gradient in x)
3) 0.000        0      # dsky/dy (sky gradient in y)
Z) 0          0      # leave in [1] or subtract [0] this comp from data?

```

A.3. Output of galfit

First group of output is the fitting of two components (images), second group with only one component. Coordinates shown in curly brackets are the coordinates and their errors according to [4]. In our analysis, the variables/errors are interpreted as uncorrelated, so that a simple propagation of error formula can be used.

```
Input image      : new_cutscale8.fits [1:60,1:60]
Init. par. file  : galfit.input
Restart file    : galfit.02
Output image     : new2_cutscale8.fits

psf      : (29.69, 24.71)   19.20
           (0.05, 0.08)    0.02
psf      : (31.11, 31.16)   17.50
           (0.01, 0.01)    0.00
sky      : [30.50, 30.50]   1.72    0.00e+00  0.00e+00
           0.00    0.00e+00  0.00e+00
Chi^2 = 160040.84238, ndof = 3593
Chi^2/nu = 44.542
```

```
Input image      : new_cutscale8.fits [1:60,1:60]
Init. par. file  : galfit_onesource.input
Restart file    : galfit.03
Output image     : newOne_cutscale8.fits

psf      : (30.93, 30.48)   17.37
           (0.01, 0.01)    0.00
sky      : [30.50, 30.50]   1.76    0.00e+00  0.00e+00
           0.01    0.00e+00  0.00e+00
Chi^2 = 365406.61697, ndof = 3596
Chi^2/nu = 101.615
```

A.4. Raw data of time delay estimate

HJD	seeing ["]	mag A	σ_A	mag B	σ_B	mag star #5	$\sigma_{star\#5}$
3 133.412	1.5	0.273	0.006	2.244	0.016	-0.175	0.013
3 134.362	1.1	0.291	0.002	2.241	0.011	-0.166	0.004
3 135.385	0.9	0.282	0.004	2.268	0.012	-0.177	0.008
3 142.386	1.3	0.287	0.002	2.273	0.007	-0.167	0.003
3 146.415	1.2	0.276	0.001	2.264	0.006	-0.178	0.002
3 150.406	0.9	0.264	0.001	2.300	0.006	-0.176	0.001
3 152.367	1.0	0.279	0.004	2.231	0.011	-0.172	0.008
3 154.407	0.9	0.267	0.002	2.252	0.007	-0.175	0.003
3 159.364	1.1	0.253	0.003	2.254	0.018	-0.174	0.005
3 163.315	1.7	0.249	0.002	2.301	0.010	-0.173	0.003
3 166.425	1.0	0.248	0.002	2.244	0.008	-0.177	0.003
3 169.393	1.1	0.222	0.003	2.317	0.011	-0.189	0.006
3 171.430	1.5	0.234	0.002	2.284	0.008	-0.172	0.004
3 173.298	1.1	0.233	0.001	2.275	0.006	-0.168	0.002
3 175.300	1.1	0.230	0.001	2.279	0.006	-0.178	0.001
3 189.265	1.1	0.208	0.007	2.236	0.023	-0.172	0.012
3 191.360	1.1	0.215	0.003	2.255	0.018	-0.167	0.004
3 193.304	1.3	0.194	0.006	2.246	0.018	-0.166	0.012
3 195.252	1.0	0.217	0.002	2.239	0.007	-0.170	0.004
3 203.314*	1.4	0.186	0.001	2.345	0.007	-0.173	0.002
3 209.256	1.0	0.189	0.003	2.198	0.010	-0.167	0.007
3 213.256	1.0	0.166	0.003	2.190	0.010	-0.183	0.007
3 216.310	1.7	0.149	0.006	2.189	0.018	-0.163	0.011
3 219.281	1.6	0.151	0.004	2.198	0.018	-0.155	0.008
3 221.234	1.0	0.178	0.002	2.241	0.009	-0.179	0.003
3 224.209	1.2	0.140	0.005	2.228	0.015	-0.166	0.010
3 232.187	1.1	0.215	0.003	2.198	0.009	-0.168	0.005
3 246.163	1.3	0.133	0.013	2.148	0.035	-0.142	0.026
3 248.138*	1.5	0.172	0.004	2.054	0.013	-0.114	0.007
3 254.125	0.9	0.156	0.004	2.139	0.013	-0.160	0.007
3 256.135	1.0	0.188	0.001	2.181	0.005	-0.173	0.003
3 261.115	1.5	0.203	0.011	2.153	0.029	-0.178	0.017
3 271.109	1.3	0.191	0.005	2.167	0.014	-0.183	0.009
3 273.103	1.2	0.163	0.007	2.117	0.020	-0.176	0.013
3 277.104	1.0	0.190	0.004	2.179	0.014	-0.191	0.007
3 281.106	1.4	0.146	0.006	2.151	0.016	-0.167	0.011
3 283.100	1.2	0.146	0.004	2.129	0.012	-0.164	0.008
3 430.540	0.9	0.167	0.002	2.078	0.009	-0.135	0.003
3 434.546	0.8	0.175	0.007	2.088	0.019	-0.143	0.009
3 461.499	0.9	0.166	0.003	2.138	0.009	-0.150	0.005

Table A.1.: Photometry of SDSS1650 and of reference star #5, as in Fig. 1.14. The Julian date corresponds to HJD-2 450 000 days. The five points marked by an asterisk are not used in the determination of the time delay.

HJD	seeing ["]	mag A	σ_A	mag B	σ_B	mag star #5	$\sigma_{star\#5}$
3 475.491	0.9	0.175	0.004	2.120	0.012	-0.179	0.008
3 482.443	1.1	0.177	0.002	2.124	0.011	-0.149	0.004
3 500.415	1.3	0.206	0.004	2.147	0.011	-0.168	0.008
3 507.348	1.0	0.177	0.005	2.106	0.012	-0.153	0.009
3 508.403*	0.9	0.199	0.003	2.222	0.009	-0.171	0.006
3 511.303	1.0	0.172	0.007	2.153	0.018	-0.151	0.012
3 517.383	0.8	0.163	0.004	2.146	0.012	-0.168	0.007
3 524.391	0.9	0.194	0.002	2.118	0.006	-0.183	0.003
3 533.412*	1.6	0.193	0.002	2.002	0.007	-0.171	0.004
3 540.345	1.0	0.194	0.003	2.124	0.011	-0.168	0.006
3 542.323	1.1	0.172	0.007	2.132	0.020	-0.194	0.014
3 552.291	0.9	0.201	0.001	2.149	0.005	-0.179	0.001
3 556.295	0.9	0.204	0.003	2.185	0.008	-0.176	0.005
3 559.280	1.0	0.181	0.002	2.134	0.007	-0.160	0.004
3 564.295*	1.3	0.228	0.001	2.300	0.007	-0.167	0.003
3 570.247	1.0	0.192	0.005	2.094	0.015	-0.165	0.010
3 575.323	1.3	0.198	0.010	2.084	0.026	-0.172	0.019
3 576.264	1.0	0.211	0.001	2.195	0.008	-0.181	0.002
3 578.275	1.2	0.189	0.002	2.133	0.007	-0.177	0.003
3 581.284	1.2	0.190	0.005	2.176	0.012	-0.188	0.009
3 611.225	1.2	0.188	0.003	2.161	0.008	-0.165	0.005
3 613.201	1.5	0.175	0.007	2.156	0.018	-0.180	0.013

A.5. Input parameters of program tdel

parameter	value
Delay_guess	30
Delay_Min	10
Delay_Max	50
Delay_nbin	10
mmag_Max	-2.5
mmag_Min	2.5
mmag_nbin	50
UseMC	0
NMC	0
MinGapLength	100

Table A.2.: Initial content of tdel.param. Some other inputs are not shown here, since they remain unchanged from default values. Later Monte Carlo is turned on with UseMC 1 and NMC 500.

A.6. Raw data of Monte Carlo

time delay[days]	probability
30.5613	0.054 704 7
31.3402	0.070 794 3
32.119	0.119 063
32.8979	0.189 858
33.6767	0.205 947
34.4556	0.186 64
35.2344	0.160 896
36.0133	0.112 627
36.7921	0.074 012 3
37.5709	0.022 525 5
38.3498	0.054 704 7
39.1286	0.016 089 6
39.9075	0.006 435 85
40.6863	0.003 217 92
41.4652	0
42.244	0.003 217 92
43.0229	0
43.8017	0
44.5806	0.003 217 92
45.3594	0

Table A.3.: Output of Monte Carlo method

Bibliography

- [1] Unknown. *Advanced lab course in physics at Bonn University: Optical Astronomy and Gravitational Lensing*. 2020.
- [2] Edward W. Kolb and Michael S. Turner. *The Early Universe*. Addison-Wesley, 1993.
- [3] P. Schneider. *Introduction to Gravitational Lensing and Cosmology*.
- [4] Chien Y. Peng. *GALFIT USER'S MANUAL*. URL: <https://users.obs.carnegiescience.edu/peng/work/galfit/README.pdf>.
- [5] C. Vuissoz et al. “COSMOGRAIL: the COSmological MOnitoringof GRAVItational Lenses”. In: (2006).
- [6] Planck Collaboration et al. *Planck 2015 results. XIII. Cosmological parameters*. 2015. arXiv: 1502.01589 [astro-ph.CO].
- [7] *AIfA 50cm Telescope: Users Manual*. 2013.
- [8] Robert J J Grand et al. “The effects of dynamical substructure on Milky Way mass estimates from the high-velocity tail of the local stellar halo”. In: *Monthly Notices of the Royal Astronomical Society: Letters* 487.1 (June 2019), pp. L72–L76. ISSN: 1745-3933. DOI: 10.1093/mnrasl/slz092. URL: <http://dx.doi.org/10.1093/mnrasl/slz092>.